Observations of Hurricane-Generated, Near-Inertial Slope Modes*

D. Y. LAI AND T. B. SANFORD

Applied Physics Laboratory and School of Oceanography, College of Ocean and Fishery Sciences, University of Washington, Seattle, WA 98105

(Manuscript received 17 June 1985, in final form 26 August 1985)

ABSTRACT

Velocity profiles and current meter measurements taken near Site D (39°10′N, 70°00′W) on the continental rise south of New England are used to study the variability of the near-inertial wave field along a sloping bottom. While the typical vertical scales of the waves are on the order of 100 m, some energetic downward propagating near-inertial features are observed with unusually large vertical scales, on the order of the ocean depth. Comparison with an internal wave model on a linear bottom slope shows that these energetic waves are dominated by the lowest three downward and seaward propagating dynamical "slope" modes. The lowest mode arrives first at Site D from the north; the higher modes follow several days later.

The observed scales and propagation directions suggest that the energetic near-inertial waves were generated by a hurricane and then reflected at the steep continental slope to the north of Site D. The low-order, flat-bottom modes that usually dominate the far-field response of a hurricane are changed by the sloping bottom into "slope" modes, which then propagate toward deeper water. Energy intensification of these modes toward the bottom suggests that sloping bottoms may play a significant role in the near-inertial wave field below the main thermocline.

1. Introduction

Near-inertial frequency motions are ubiquitous in the ocean (Fu, 1981) and account for a substantial portion of the internal wave energy. Most of the observed horizontal and vertical coherence scales of these waves are small in the thermocline and deep ocean (Webster, 1968; Fu, 1981). One exception to these scales is energetic near-inertial waves produced in the surface mixed layer by moving wind stress (Pollard, 1980). Such energy can be transferred rapidly to the main thermocline via inertial pumping at the bottom of the mixed layer (Price 1983, 1986). As a result, energetic inertial motions in the main thermocline have large vertical scales within several inertial periods after the forcing. This kind of inertial motion has been observed after the passage of atmospheric fronts and hurricanes (Brooks, 1983; D'Asaro, 1984; Shay and Elsberry, 1986). Price (1983) also shows that the far-field response to a hurricane is dominated by low modes as they propagate rapidly away from the source. Few measurements are available to reveal the far-field response.

Far-field response to a hurricane in the presence of a sloping bottom is investigated in this paper. Observations of near-inertial motions are provided by electromagnetic velocity profiles (EMVP hereafter; Sanford et al., 1978) and current meters. They were taken over a period of a month near Site D on the continental rise south of New England. Two hurricanes passed by the area during this period. "Slope" modes are introduced in a model of near-inertial waves on a sloping bottom. The relationship between the slope modes, the hurricanes and the observed energetic near-inertial motions are examined.

2. The data

Site D is situated at 39°10′N, 70°00′W, on the continental rise south of New England with a water depth of 2700 m and a bottom slope of about 0.01. From 22 August through 14 September 1972, a series of EMVPs was taken, for the most part within a small area around Site D (Figs. 1 and 2).

Profiling was interrupted twice by the approach of Hurricanes Carrie and Dawn. Consequently the profiles are categorized into three groups (Figs. 1 and 2). Group A profiles, taken 22–31 August before the appearance of Carrie, presumably represent the ambient oceanic conditions near Site D in the absence of intense, local atmospheric forcing. Group B profiles, spanning about 2 days, were obtained 2 days after Carrie passed over the region. The rest of the profiles (Group C) were taken 3 days after the closest approach of Dawn. There are gaps of 4–5 days between the groups during which no profiles were taken because R/V *Gosnold* returned to port to avoid the hurricanes.

Long-term current meter moorings were maintained near Site D by the Woods Hole Oceanographic Institution. Five moorings were in operation during Group

* School of Oceanography Contribution No. 1453.

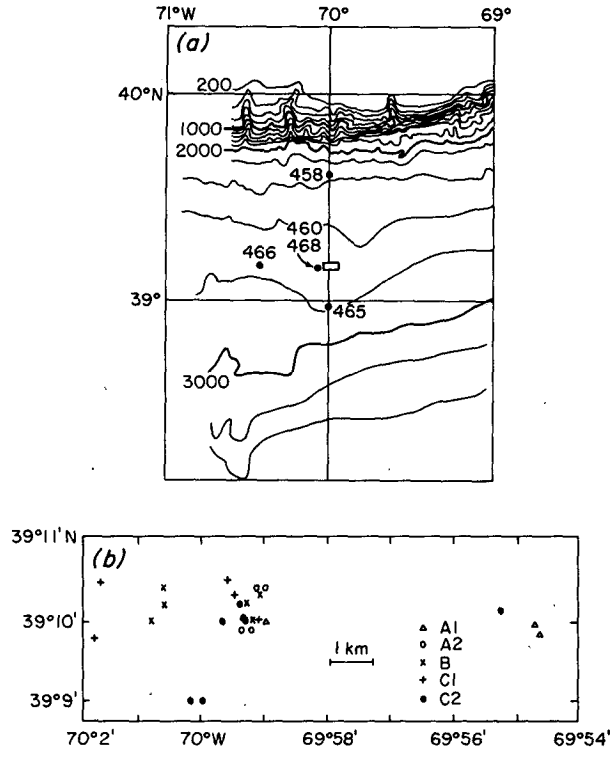

FIG. 1. Locations of current meter moorings and EMVPs. Moorings (panel a) are identified by dots with three digit numbers. Also shown are bottom contours (in meters) of the region. The rectangle represents the chart area shown in panel b. Different symbols identify the individual EMVPs that make up the near-inertial profiles.

B and C profiling. They extend from the bottom of the continental slope to the north, to 20 km south and 40 km west of Site D (Fig. 1a). In all, eight current meters were on these moorings, providing current measurements from a 985-m depth to near the bottom (Table 1).

The EMVPs provide detailed observations of horizontal currents in the vertical but at limited points in time. The current meters provide observations over time, albeit at limited points in the vertical. Combination of the two sets of observations presents a distinct view of oceanic motions which would not be available with just one type of measurement.

3. Near-inertial motions

a. Demodulation analysis

To resolve more clearly the time- and depth-dependence of the near-inertial motions, a demodulation technique is applied to both the current meter and EMVP measurements. It is similar to the methods used by Rossby and Sanford (1976) and Perkins (1976).

Current meter measurements are divided into shorter segments of two inertial periods (37 hours in this case). Each segment is least-square-fitted at a chosen near-inertial frequency after the mean is subtracted. Consecutive segments are overlapped by 50%. The amplitude and phase computed from the coefficients represent the near-inertial motions during the time segment.

The EMVPs taken within two inertial periods (37 hours) and with a maximum separation of 7 km are grouped together for the demodulation, which is done independently at each depth. The mean of velocity measurements at each depth for each group is removed before the least-square-fitting. Five profiles of near-inertial oscillations are obtained (Table 2). Two profiles (A1 and A2) are computed for Group A, one for Group B and two for Group C (C1 and C2). While 7 km separation is the grouping criterion for the profiles, the average separation between profiles is less than half of that (Fig. 1b). A discussion of the analysis error is presented in the Appendix.

The demodulation frequency used in both cases is 3% above the local inertial frequency. It is chosen because the fitted phase does not change with time during 7–13 September (Fig. 2), indicating that it is the dominant frequency (Perkins, 1976).

b. EMVP observations

Figure 3 shows the amplitude and phase profiles of the demodulated near-inertial motions. The phases are computed with respect to a common time origin. Group A and B profiles are similar. Their amplitudes are small (1–2 cm s^{-1}), and both exhibit large fluctuations of phase within depth intervals of 100–500 m.

Group C profiles differ substantially from Groups A and B. Energy in Group C is more than three times that of the earlier period (Table 2) and is observed throughout the water column of 2700 m. There is a striking difference in the phase variations with depth. Group C profiles show a markedly linear increase of phase with depth, especially from −1000 to −2000 m. This indicates that the energetic near-inertial motions are dominated by downward propagating waves of large vertical wavelengths (Leaman and Sanford, 1975).

Downward energy propagation is also suggested by the downward movement of the energy maximum and minimum below the main thermocline in Group C profiles. The maximum and minimum amplitudes near −2000 m moved down by 200 m from C1 to C2 (Fig. 3b). The difference in the average drop times between the profiles that constituted the near-inertial profiles C1 and C2 is 41 hours. This yields a downward vertical group velocity of 120 m day^{-1} if the relocation of the maximum and minimum in the vertical is assumed solely due to the downward movement of the wave-packet.

c. Current meter observations

The EMVP data are complemented by current meter measurements. Most of the current meter records show

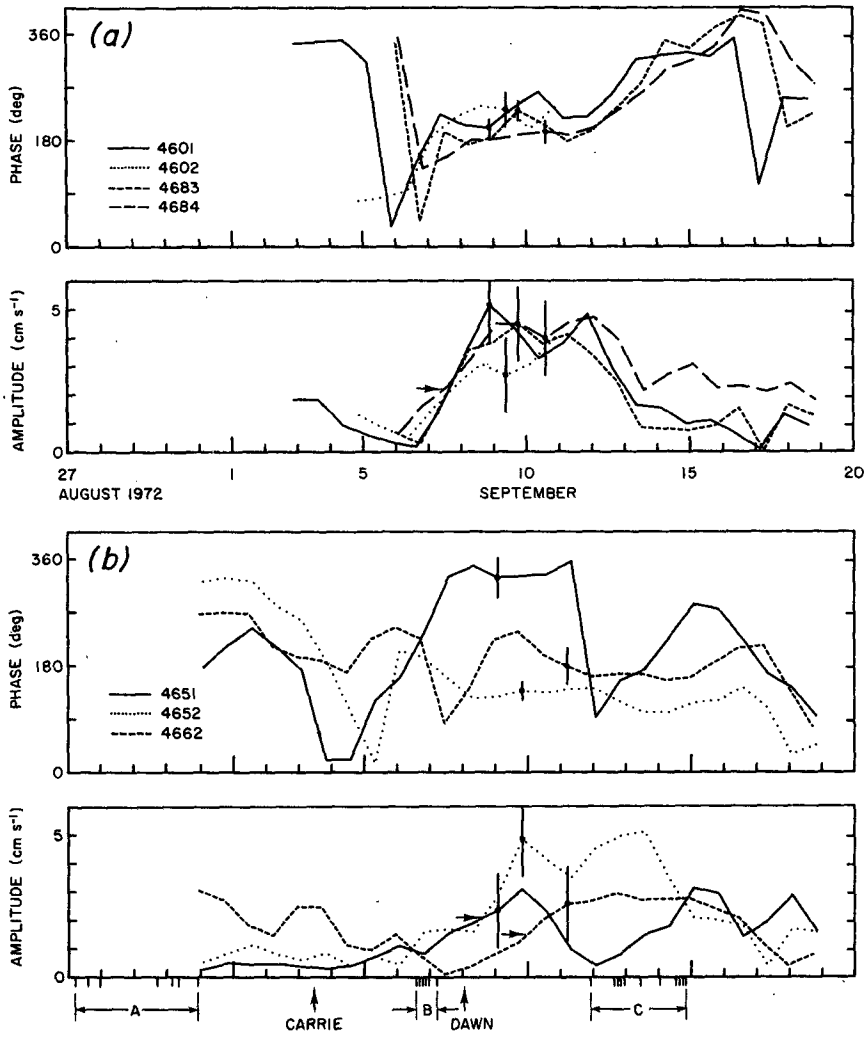

FIG. 2. Amplitudes and phases of demodulated near-inertial motions from current meters. The phases shown are computed with respect to a common time origin. The demodulated frequency used is 3% above the local inertial frequency. Figure 2a is from near-bottom current meters within 10 km of Site D. Figure 2b is from current meters farther away from Site D. Selected 90% confidence limits are indicated by the vertical bars. They are calculated using the error model described in the Appendix. The horizontal arrows indicate the ambient energy level of each record and the estimated times of arrival of the energetic features. Deployment times of the EMVPs are indicated by ticks below the time axis. The times of the closest approaches of Hurricanes Carrie and Dawn, and the EMVP groups are shown.

that energetic near-inertial motions are present not only during the deployment of the Group C profiles but also several days before (7–11 September) (Fig. 2). Record 4581 (not shown), at the bottom of the continental slope, has no energetic motions during the same period.

During 7–11 September, there is no significant phase difference in the bottom 300 m (moorings 460 and 468) (Fig. 2a). A phase difference of 180° is found between −1000 m and the bottom on mooring 465 (Fig. 2b). It deviates from 180° after 11 September. This is also the time when the Group C profiles were taken (11–14 September). The significance of the 180° phase difference and its evolution in time will be discussed in section 4b.

It is difficult to identify the exact arrival times of the energetic near-inertial motions at the various moorings because of the limited horizontal coverage of the array and the uncertainty in choosing a background energy level. If the record-averaged near-inertial energy of each series is chosen to be the ambient energy level (marked by horizontal arrows in Fig. 2), it appears that the energetic motions arrived at moorings 460 and 468 about 1 day earlier than at 465 which is 20 km to the south. This suggests a southward energy propagation of 20

TABLE 1. Tabulation of current meter records. A mooring is designated by a three digit number. An instrument is designated by appending a digit to the mooring number; lowest numbers are closest to the surface.

Mooring number	Location	Water depth (m)	Record number	Instrument depth (m)
458	39°36.6'N 70°00.2'W	2263	4581	−1963
460	39°09.8'N 70°03.9'W	2664	4601	−2363
			4602	−2564
465	38°59.0'N 70°00.0'W	2756	4651	−985
			4652	−2487
466	39°09.2'N 70°30.8'W	2748	4662	−1980
468	39°10.0'N 70°02.8'W	2666	4683	−2364
			4684	−2564

km day^{-1}. Indication of a westward propagation component is provided by the delay in the arrival of energetic motions at instrument 4662 to the west, although this interpretation is weakened by the depth differences between this single current meter and the instruments at other moorings.

Further evidence of southward energy propagation is provided by the phases of the near-inertial current near the bottom. During 8–11 September, phase increases significantly by 60° to 90° from current meter 4652 northward toward instruments at the same depth on moorings 460 and 468 (Fig. 2). In our convention, this means a southward phase propagation, and hence southward energy propagation.

4. Near-inertial waves on a slope

There is evidence that internal wave fields near topographic features differ significantly from the canonical model of Garrett and Munk (1972). Wunsch (1976) observes sharp increases of high frequency internal wave energy near the Muir Seamount. Eriksen (1982)

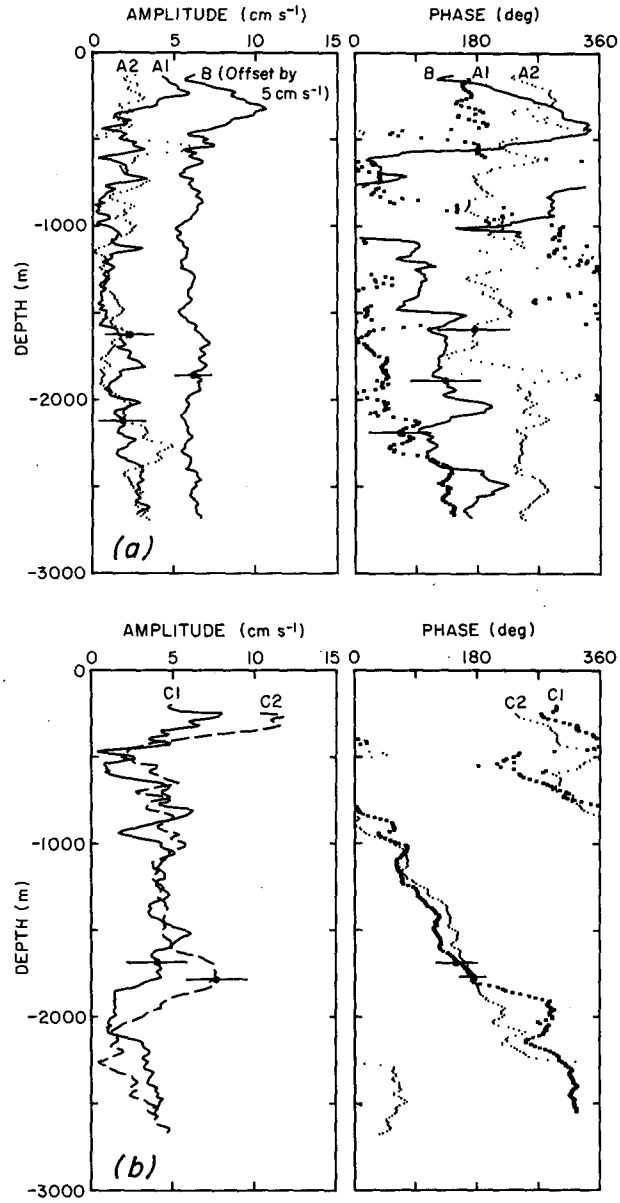

FIG. 3. Amplitude and phase of (a) Groups A and B, and (b) Group C near-inertial profiles. The phases shown are computed with respect to a common time origin. A1 and A2 are obtained from subgroups within Group A profiles. The amplitude for B is offset by 5 cm s^{-1} for clarity. C1 and C2 are subgroups within Group C profiles. The 90% confidence limits are indicated by the horizontal bars. They are calculated using the error model described in the Appendix.

TABLE 2. Depth-averaged kinetic energy for the near-inertial profiles A, B and C, which are further separated into subgroups A1, A2, etc. The numbers of individual profiles that made up the subgroups, the maximum horizontal separation among the profiles and the time duration spanned in each subgroup are listed.

Near-inertial profile	Number of individual profiles	Maximum separation (km)	Duration (hours)	Depth-averaged kinetic energy (J m^{-3})
A1	3	6	19	0.25
A2	4	1	30	0.28
B	6	2	12	0.15
C1	5	3	24	0.80
C2	7	7	33	1.20

shows that polarization and intensification of internal waves occur at frequencies near the critical value as the waves reflect off sloping bottoms.

While Eriksen's model is best suited to study the effects of sloping bottoms on short waves many wavelengths away from the surface, long waves, such as those observed after 7 September, necessarily "feel" the bottom and are more appropriately represented as vertical

modes. The effects of the sloping bottom on the near-inertial waves are discussed below in terms of vertical modes. The model presented is similar to that of Wunsch (1969) except for the inclusion of the Coriolis parameter.

a. The sloping bottom model

Consider a semi-infinite domain bounded above by a rigid surface and below by a bottom with a linear slope of α. The linearized perturbation equations for an inviscid, stably stratified Boussinesq fluid are

$$u_t - fv = -\frac{P_x}{\rho_0} \tag{1}$$

$$v_t + fu = -\frac{P_y}{\rho_0} \tag{2}$$

$$w_{tt} + N^2 w = -\frac{P_{zt}}{\rho_0} \tag{3}$$

$$u_x + v_y + w_z = 0, \tag{4}$$

where notations are standard, and z is positive upward.

For a two-dimensional case ($z = -\alpha x$ and $\partial/\partial y = 0$), one can introduce a streamfunction $\hat{\psi}$ with $u = -\hat{\psi}_z$ and $w = \hat{\psi}_x$. If we assume a periodic motion at frequency ω such that

$$\hat{\psi} = \psi \exp(-i\omega t),$$

then the equations can be reduced to

$$\psi_{zz} - c^{-2}\psi_{xx} = 0 \tag{5}$$

with

$$c^2 = \frac{\omega^2 - f^2}{N^2 - \omega^2}.$$

The boundary conditions are

$$\psi = 0 \quad \text{at} \quad z = 0 \quad \text{and} \quad -\alpha x. \tag{6}$$

Propagation of internal waves along a sloping bottom is determined by c, the slope of the wave characteristics, and α. For a subcritical slope in which $\alpha < c$, waves can propagate up and down the slope. Waves cannot move up a supercritical slope ($\alpha > c$) as they are reflected off the bottom back into deeper water.

Unlike the case of a flat-bottom ocean, Eq. (5) is not separable. Let us consider the case of a subcritical slope, $\alpha < c$, which is pertinent to inertial–internal wave motions at Site D. Exact solutions exist for a constant N (Wunsch, 1968, 1969; Manton and Mysak, 1971). The propagating wave solutions for (5) are

$$\psi_+ = \exp[iq \ln(cx - z)] - \exp[iq \ln(cx + z)] \tag{7}$$

and

$$\psi_- = \exp[-iq \ln(cx - z)] - \exp[-iq \ln(cx + z)], \tag{8}$$

where

$$q = 2n\pi \Big/ \ln\left(\frac{c + \alpha}{c - \alpha}\right)$$

and n is the mode number. The horizontal velocities corresponding to ψ are

$$u = -\psi_z; \quad v = -iu(f/\omega).$$

The components are combined to form $V(x, z)e^{i\theta(x,z)}$ where V and θ are the amplitude and phase functions respectively.

These slope modes are not simple plane waves; they are dependent on their locations [Eqs. (7) and (8)]. The V and θ of the lowest three V_+ modes (corresponding to ψ_+) at Site D for a near-inertial frequency of $1.03f$ are shown (Fig. 4c, d). Values representative of those at Site D are used for the computation ($N = 1.6 \times 10^{-3}$ s^{-1}, $\alpha = 10^{-2}$, and a water depth of 2700 m).

The vertical wavenumber of these modes and their energy increase toward the bottom (Fig. 4c, d). The group velocity of each mode is obtained by dividing the energy flux by the energy density, both of which can be computed directly from (1)–(4). These V_+ modes propagate energy seaward and downward (Table 3). The phase of each mode increases with depth, consistent with the downward energy propagation.

Amplitudes of the V_- modes are similar to those of the V_+, but their phases decrease with depth as a result of the opposite energy propagation direction (shoreward and upward).

b. Comparison with observations

The energetic near-inertial profiles appear to have characteristics similar to those of the lowest V_+ modes; their phases increase monotonically with depth, and there are several energy maxima and minima in the vertical. To compare the data with the modes more closely, the near-inertial profiles are WKB-scaled using the vertically averaged Väisälä frequency (0.91 cph) as the normalization factor N_0. This results in a scaled depth range the same as the original depth of 2700 m (Fig. 4a, b). These profiles are least-square-fitted to a set of modes, starting with only the lowest mode. Fitting is then repeated several times, increasing the number of modes used by one each time; the additional mode is always the next higher mode. For example, the third fit was done using the first, second and third modes.

The same fitting procedure is done using sets of V_+, V_- and flat-bottom dynamical modes (Fjeldstad, 1933) separately. Although the first two sets of modes satisfy the sloping bottom boundary condition, the flat-bottom modes do not. The data are fitted to the latter for comparison.

The V_+ modes best describe the large vertical scales in the energetic near-inertial motions. More than 75% of the observed energy can be attributed to the lowest

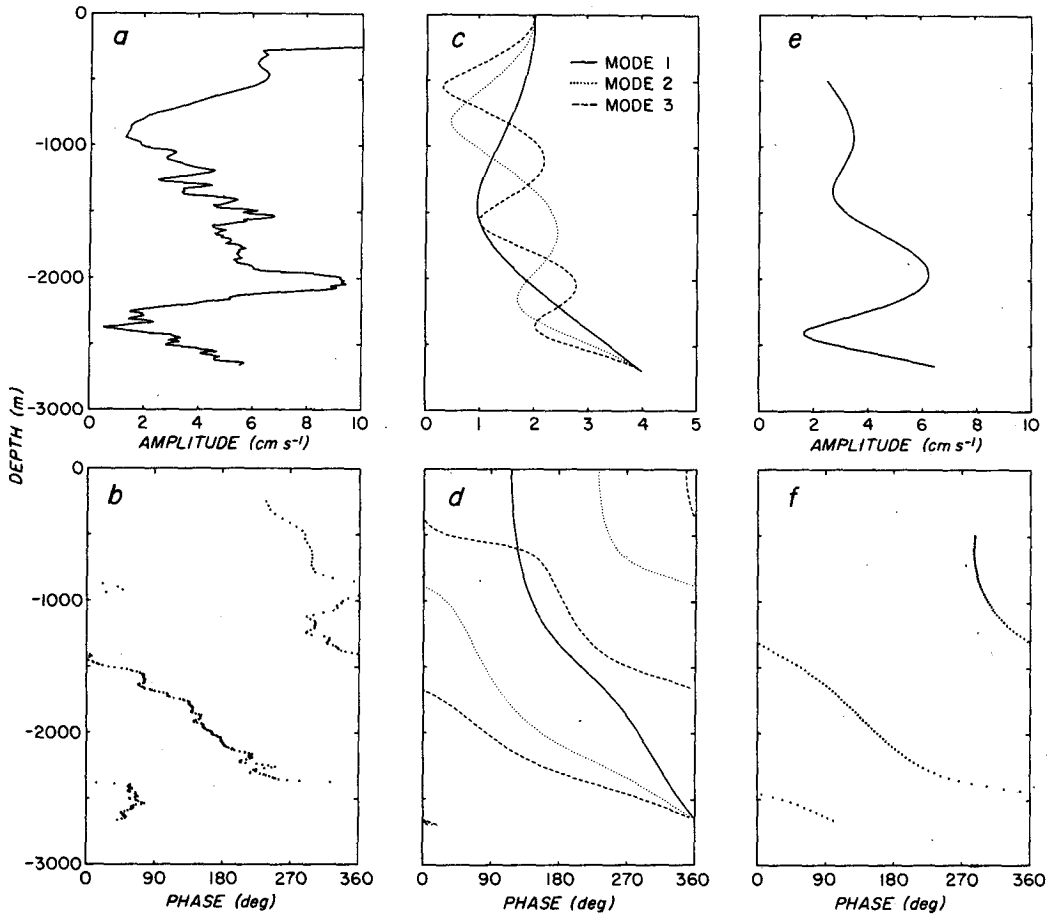

FIG. 4. Amplitudes (V) and phases (θ) of the observed energetic WKB-scaled near-inertial profiles (a and b), each of the three theoretical downward and seaward "slope" modes (V_+) (c and d) at Site D, and the sum of the three fitted modes (e and f). Increasing phase with depth means downward energy propagation. Normalization of the scaled profile is done using the vertically averaged Väisälä frequency (0.91 cph) so that the depth of the scaled ocean is the same as the original. The amplitudes of the modes in panel c have been scaled by the square root of the vertically averaged kinetic energy.

three V_+ modes (Fig. 5). This percentage is much higher than that of the other two sets. The energy density and flux of these three observed V_+ modes are given in Table 3.

While the V_- modes do not account for the energetic motions very well (Fig. 5), the flat-bottom modes describe the motions rather well when more than five modes are used for the fitting. This is an artifact of mode-fitting; any set of reasonable functions (modes), although they do not satisfy the dynamics, can describe the motions well if enough modes are used.

The dominance of the lowest three V_+ modes in the energetic motions is consistent with the current meter measurements. During 7–11 September before Group

TABLE 3. Energy density, energy flux and group velocity of the first three observed V_+ modes at Site D for $\omega = 1.03f$. The first two quantities are computed from the mode-fitting of the WKB-scaled near-inertial profile C2 to theoretical modes. The normalization factor used here for the scaling is 0.91 cph. Group velocity is the ratio of the flux and density, and is independent of the fitted results; it is calculated directly from Eqs. (1)–(4).

		Energy flux		Group velocity	
V_+ mode number	Energy density (J m^{-3})	North (10^{-3} J m^{-2} s^{-1})	Vertical (10^{-3} J m^{-2} s^{-1})	North (km day^{-1})	Vertical (m day^{-1})
1	0.24	−59	−0.37	−21	−130
2	0.18	−22	−0.14	−10	−67
3	0.33	−27	−0.17	−7	−45

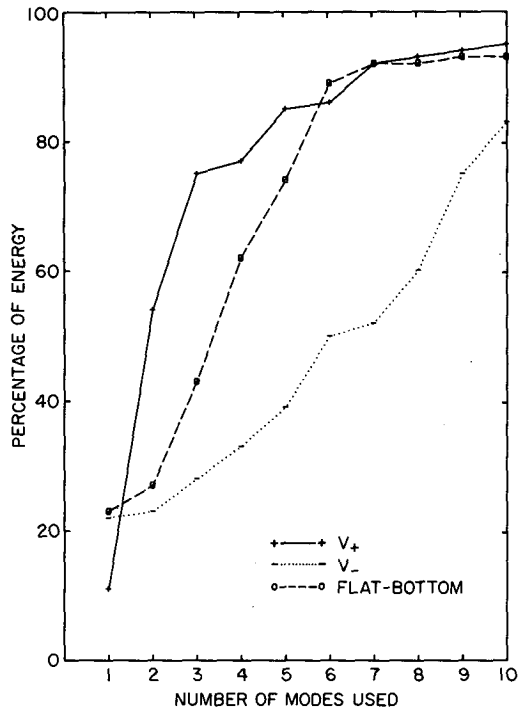

FIG. 5. Results of mode fitting using V_+, V_- and flat-bottom modes, respectively. Percentages of near-inertial energy accounted for are plotted against the number of modes used in the fitting.

C profiles were taken, current meter records on mooring 465 show a phase difference of 180° in the near-inertial motions between −1000 and −2500 m (Fig. 2b). This phase difference is a characteristic of the first V_+ mode[1] (Fig. 4d), suggesting the presence of only the first mode during this period. The observed southward energy propagation of 20 km day^{-1} during 7–8 September (section 3c) agrees well with the group velocity of the first V_+ mode (Table 3). The deviation of the phase difference from 180° after 11 September suggests the arrival of more modes in the second half of the observation period (Fig. 2b), in qualitative agreement with the EMVP observations.

It is important to point out that while a 180° phase change in the vertical is also a characteristic of the first flat-bottom mode, the zero crossing of this mode at Site D is at −700 m. If this flat-bottom mode were dominant from 7–11 September, the observed phase difference between −1000 and −2500 m would have been zero.

Similar mode-fitting is done with the ambient near-inertial motions observed in Group A and B profiles. Only 50% of the energy can be accounted for by the lowest three V_+ modes.

[1] Figure 2b shows that the observed phases at two depths decrease by 180° with depth while the opposite is true for the first V_+ mode (Fig. 4d). This discrepancy is an artifact of the "360° ambiguity" of phases or angles.

The above analysis shows that observed energetic near-inertial motions near Site D during 7–14 September can be attributed to the presence of the lowest three V_+ modes. The vertical and horizontal energy propagation directions of these modes are consistent with those observed. The first V_+ mode arrives at moorings 460 and 468 on 7 September from the north, and at mooring 465 a day later. It is followed 4 days later by the second and third modes. In the next section we will explore possible generation mechanisms of these waves.

5. Discussion

a. Atmospheric forcing

Many observations have shown that surface forcing by storms, hurricanes and atmospheric fronts is a potent source of near-inertial motions observed in the main thermocline (Brooks, 1983; D'Asaro, 1984; Shay and Elsberry, 1985). The energetic poststorm motions tend to have large vertical scales, and the observed energetic near-inertial motions at Site D have this characteristic.

Price (1983) studied the oceanic response to a moving hurricane using a numerical model. He shows a right-biased intensification in the posthurricane near-inertial velocity field, due to the coupling of the clockwise rotation of the wind vector at fixed points to the right of the hurricane (looking along the direction of the hurricane track) with the preferred rotation of oceanic inertial motions in the Northern Hemisphere. In the main thermocline, the maximum velocity response occurs several hurricane radii to the right of the hurricane track; there is a minimum response directly under the track. Divergence of the near-inertial motions in the surface mixed layer results in inertial pumping at the base of the mixed layer, which causes rapid energy transfer in the vertical. As a result, within several inertial periods after the forcing, near-inertial motions are dominated by waves with large vertical scales on the order of the ocean depth. Low modes are found in the far field as they propagate out of the forced region.

Two hurricanes approached Site D during the experiment (Figs. 2 and 6). Hurricane Carrie traveled northward toward New England and passed almost directly over Site D on 3 September. Its maximum wind speed was 50 knots. Less than a week later Hurricane Dawn approached Site D from the south. On 8 September it turned westward, and its center came within 300 km south of Site D. While Dawn's maximum wind reached 40 knots, wind observed at Site D during its closest approach was only 10 knots (Peter Black, personal communication, 1984).

The observed near-inertial energy levels begin to rise at about the time of the closest approach of the second hurricane, Dawn (Fig. 2). However, we believe that Carrie, rather than Dawn, was the primary forcing mechanism for the following reasons.

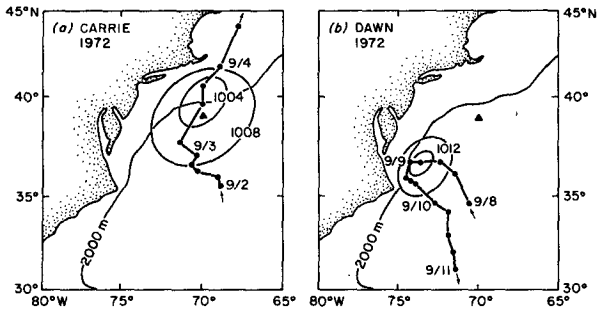

FIG. 6. Tracks of Hurricanes Carrie (a) and Dawn (b). The coastline and the 2000 m bottom contour are shown. Estimated positions of the hurricane centers are identified by solid dots every six hours. Times shown are GST. Site D is identified by a solid triangle. The atmospheric pressure fields (in millibars) due to the hurricanes at their closest approach to Site D are shown.

1) Local generation of these motions is unlikely because the wind observed at Site D is weak during the passage of Dawn.

2) It is possible that these motions are the far-field response to Dawn as the low modes, especially the first mode, propagate rapidly northward away from the forced region (Price, 1983). However, these shoreward propagating low modes would have to be affected by the sloping bottom to result in upward energy propagating V_- modes (see section 4a). These propagation directions are opposite to those observed (see sections 3b and 3c).

3) Beta-effect tends to inhibit poleward propagation of near-inertial waves, especially the high modes (Gill, 1984; Price, 1986). Dawn is a zonally propagating hurricane south of Site D. Near-inertial waves generated by Dawn would soon reach their turning latitudes as they propagate poleward. They would be reflected back toward the equator and would not have reached Site D.

The absence of a significant increase in near-inertial energy at Site D immediately after the passage of Hurricane Carrie is consistent with the minimum velocity response directly under the hurricane track as suggested by Price (1983). Carrie is strong enough to generate energetic near-inertial motions somewhere else on its path, but the motions at Site D should remain weak.

As described in section 4b, the first V_+ mode arrives at mooring 465 from the north on 8 September. It is followed by the second and third modes 4 days later. If we assume that the different arrival times are due to the different southward group velocities of the first two modes (C_{g1} and C_{g2}) in the 2-D model presented in section 4a (Table 3), and that the modes are generated at the same time and same place, the generation location and time of these waves can be calculated.

Let t_1 and t_2 be the times of arrival of modes 1 and 2 at mooring 465, and t_0 and d the generation time and the distance of the generation location from this mooring, respectively. Then

$$t_1 - t_0 = d/C_{g1} \quad \text{and} \quad t_2 - t_0 = d/C_{g2}. \tag{9}$$

This leads to

$$d = \frac{(t_2 - t_1)C_{g1}C_{g2}}{C_{g1} - C_{g2}}. \tag{10}$$

Substituting appropriate values (Table 3) into (9) and (10) yields

$$d = 80 \text{ km}, \quad t_1 - t_0 = 4 \text{ days} \quad \text{and} \quad t_2 - t_0 = 8 \text{ days}.$$

Thus the modes were generated 80 km north of mooring 465 (60 km north of Site D). It takes 4 days for the first mode to arrive at mooring 465 (3 days for Site D).

The computed generation location is near the base of the continental slope where the bottom slope is steeper than 10^{-2} (Fig. 1a), making it supercritical for near-inertial waves (i.e., $\alpha > c$). Near-inertial waves generated there, or to the south, cannot penetrate such a slope and are reflected southward (seaward). The absence of energetic near-inertial motions at 458 during this period agrees qualitatively with the hypothesis, although the location of the mooring (50 km north of Site D) suggests that reflection might have occurred slightly south of what has been calculated. Other current meter observations at the same location at other times show that the inertial energy there is almost an order of magnitude lower than that on the continental rise (Wunsch and Hendry, 1972), which also suggests the reflection of these motions at the supercritical slope.

The above calculations show that the first two modes and Hurricane Carrie were in the same vicinity on the continental slope at the same time (to within a day)[2] (Figs. 2 and 6). Their coincidental presence, large vertical scales and propagation direction, all suggest that the energetic near-inertial motions observed near Site D are generated by Carrie to the north. These waves would have propagated northward (in the same direction as the hurricane track) in a normal wake (Price, 1983). The presence of the supercritical slope forces them to go southward.

b. *Other possible mechanisms*

While evidence suggests that the energetic near-inertial motions at Site D are generated by a hurricane, other mechanisms cannot be excluded. They are discussed here.

During the experiment, an anticyclonic warm Gulf Stream ring moved into the region. Large northward currents are observed in some of the Group B and all of the Group C profiles. The strong current shear of the ring extends from the surface to −500 m.

[2] This one-day difference is attributed to the uncertainty in the estimated times of arrival of the energetic features. A small reduction of 0.5 cm s^{-1} in the record-averaged energy (from which the times of arrival are estimated) would put the first two modes and the hurricane at the same place at exactly the same time.

The presence of the warm ring at Site D could support the argument that the energetic near-inertial motions observed are related to the strong current. Kunze (1985) suggests that trapping and intensification of near-inertial motions can be found on the negative vorticity side of a mean shear current. Observations in the North Pacific Subtropical Front show evidence of such a mechanism (Kunze and Sanford, 1984).

There are three reasons that argue against such a hypothesis at Site D. First, strong mean currents are observed in both Group B and C profiles, but energetic near-inertial motions are found only in the latter. Second, the strong vertical shear of the current in the warm ring is not observed below −500 m. Its presence is essential for the trapping of the energy (Kunze, 1985), and yet energetic motions are observed both above and below this depth. Finally, waves observed in this study have large vertical scales characteristic of wind-generated motions, but waves trapped by the mean current tend to have short vertical wavelengths (Kunze, 1985).

The strong current of the ring could also interact with the continental slope. Quasi-steady currents flowing over a rough or undulated bottom could generate internal waves (Bell, 1975). There is observed evidence of such a mechanism near Bermuda in the presence of a Gulf Stream ring (Johnson and Sanford, 1980). These waves propagate upward from the bottom and do not necessarily have low mode structures. Besides they would have zero Eulerian frequency. Therefore it is unlikely that mean current-topography interaction is responsible for the energetic features observed at Site D.

6. Summary and conclusion

The EMVP and current meter measurements near Site D show near-inertial motions several times more energetic than the ambient levels. These motions are dominated by large vertical scales and are observed to propagate seaward and downward. Comparison of the data with vertical dynamical "slope" modes on a sloping bottom suggests that most of the energy can be attributed to the lowest three modes. Calculations suggest that these modes come from the steeper continental slope to the north. The low-mode nature of the energetic motions, the coincidental presence of Hurricane Carrie in the computed generation region of the modes, and the subsequent arrivals of the lowest modes at Site D from the north all suggest that the latter are storm-generated near-inertial waves.

Far-field response to a hurricane is usually dominated by the lowest flat-bottom vertical modes (Price, 1983). The modification of this response by a sloping bottom is significant for the near-inertial wave field. Energy of these "slope" modes intensifies, and their vertical scales shorten toward the bottom. More energy is concentrated below the main thermocline than would be provided by the lowest flat-bottom modes. Amplification and shortening of the waves could lead to their breaking and mixing near sloping bottoms, which makes them likely sinks for the near-inertial energy.

Acknowledgments. The experiment was conducted with the assistance of J. Luyten, R. Drever, J. Dunlap, A. Bartlett, E. Denton and T. Crook. Capt. H. Seibert and the crew of R/V *Gosnold* were particularly helpful and cooperative. The current meter records were collected and processed by the Buoy Group at the Woods Hole Oceanographic Institution. We thank E. D'Asaro, E. Kunze, P. Spain, J. Price and L. Shay for their helpful comments, and T. Shay for the Väisälä frequency profile in a warm ring. Peter Black of the NOAA Hurricane Research Division kindly provided us with wind stress information on the two hurricanes. This information and his comments enabled us to detect some errors in an earlier version of this manuscript. The Office of Naval Research supported the experiment and analysis. The analysis done at the University of Washington was funded under ONR Contract N00014-84-0111.

APPENDIX

Error Analysis

For a series of velocity measurements taken over time at a given depth, from either current meters or EMVPs, the complex near-inertial velocity U_I is obtained by a demodulation method (Perkins, 1976; Rossby and Sanford, 1976). The mean current of the series is removed first. The residual velocities are least-square-fitted to a clockwise rotating vector (with time) at a chosen near-inertial frequency. Confidence limits on U_1 are computed using the following error model.

Let $\hat{U}_I$ be the true near-inertial velocity. Then

$$U_I = \hat{U}_I + \epsilon_{LF} + \epsilon_{HF},$$

where the ϵ terms are errors due to low- and high-frequency signals which are considered as noise in this computation. These errors vary depending on the energy levels of the noise and the sampling schemes of the series.

The term ϵ_{HF} is the error due to high frequency internal waves. It is estimated for each series by fitting a random internal wave field to the near-inertial frequency. The mean squared velocity of the wave field is chosen to be 44 (N/N_0) cm^2 s^{-2}, with N_0 equal to 3 cph (Garrett and Munk, 1972; Munk, 1981).

The mean velocity of each series is removed first before the demodulation. Since the chosen duration of each series is less than two inertial periods and there is little energy at such periods at Site D (Thompson, 1977), the subtraction of the mean essentially removes all the low-frequency signals from the series. Thus, error due to the actual low-frequency signals in the demodulation is negligible. However, an artificial mean could be introduced as a result of the sampling scheme. An inertial current should have a zero mean if sampled

TABLE A1. The rms differences between near-inertial amplitudes computed using different horizontal separation criteria.

Near-inertial profile	Number of individual profiles	rms difference (cm s^{-1})
A1a	2	0.87
Ba	3	0.65
C1a	3	0.60
C2a	4	0.64

perfectly (e.g., sampled equally in time over whole inertial cycles). Otherwise, the mean of the series would include the actual low frequency signals as well as an artificial mean. Removal of this mean from the series would introduce the artificial mean into the series. This would result in errors in U_I, which we call ϵ_{LF}. It is actually the error due to the presence of the artificial mean and not the actual low frequency signals.

To estimate ϵ_{LF}, an inertial current of 2 or 5 cm s^{-1} (the observed weak and energetic vertically averaged inertial velocity, respectively) (Table 2), sampled accordingly for each series, is used. The artificial mean thus obtained is used as input in the demodulation. The resultant amplitude is ϵ_{LF}, which would have been zero if the sampling were perfect.

The total variance of the inertial velocity is the sum of variances calculated from ϵ_{HF} and ϵ_{LF}, respectively. The 90% confidence limits for the amplitude of the inertial velocity are computed from a Rayleigh distribution. The confidence limits on the phases are calculated from the maximum deviations of the velocity vectors using the 90% confidence circles. Some of these computed confidence limits are shown in Figs. 2 and 3.

Errors are introduced in grouping profiles at different locations for the demodulation. To estimate the errors, a more stringent criterion for the grouping is applied; a maximum separation of only 1 km is allowed. This greatly reduces the number of profiles in each near-inertial profile. The root-mean-square differences between the modified and original near-inertial amplitudes are shown in Table A1. The differences are small compared with the amplitudes of the near-inertial currents, especially in Group C.

REFERENCES

Bell, T. H., 1975: Topographically generated internal waves in the open ocean. *J. Geophys. Res.*, **80,** 320–327.

Brooks, D. A., 1983: The wake of Hurricane Allen in the western Gulf of Mexico. *J. Phys. Oceanogr.*, **13,** 117–129.

D'Asaro, E. A., 1984: Wind forced internal waves in the North Pacific and Sargasso Sea. *J. Phys. Oceanogr.*, **14,** 781–794.

Eriksen, C. C., 1982: Observations of internal wave reflection off sloping bottoms. *J. Geophys. Res.*, **87,** 525–538.

Fjeldstad, J., 1933: Interne wellen. *Geofys. Publ.*, **10,** 1–35.

Fu, L. L., 1981: Observations and models of inertial waves in the deep ocean. *Rev. Geophys. Space Phys.*, **19,** 141–170.

Garrett, C. J. R., and W. H. Munk, 1972: Space-time scales of internal waves. *Geophys. Fluid Dyn.*, **3,** 225–264.

Gill, A. E., 1984: On the behavior of internal waves in the wakes of storms. *J. Phys. Oceanogr.*, **14,** 1129–1151.

Johnson, C. L., and T. B. Sanford, 1980: Anomalous behavior of internal gravity waves near Bermuda. *J. Phys. Oceanogr.*, **10,** 2021–2034.

Kunze, E., 1985: Near-inertial wave propagation in geostrophic shear. *J. Phys. Oceanogr.*, **15,** 544–565.

——, and T. B. Sanford, 1984: Observations of near-inertial waves in a front. *J. Phys. Oceanogr.*, **14,** 566–581.

Leaman, K. D., and T. B. Sanford, 1975: Vertical energy propagation of inertial waves: A vector analysis of velocity profiles. *J. Geophys. Res.*, **80,** 1975–1978.

Manton, M. J., and L. A. Mysak, 1971: Construction of internal wave solutions via a certain functional equation. *J. Math. Anal. Appl.*, **35,** 237–248.

Munk, W., 1981: Internal waves and small scale processes. *Evolution of Physical Oceanography: Scientific Surveys in Honor of Henry Stommel.* B. A. Warren and C. Wunsch, Eds., The MIT Press, 264–291.

Perkins, H., 1976: Observed effect of an eddy on inertial oscillations. *Deep Sea Res.*, **23,** 1037–1042.

Pollard, R. T., 1980: Properties of near-surface inertial oscillations. *J. Phys. Oceanogr.*, **10,** 385–398.

Price, J. F., 1983: Internal wave wake of a moving storm. Part 1: Scales, energy budget and observations. *J. Phys. Oceanogr.*, **13,** 949–965.

——, 1986: Internal wave wake of a moving storm. Part 2: Parameter dependence. *J. Phys. Oceanogr.* (submitted).

Rossby, H. T., and T. B. Sanford, 1976: A study of velocity profiles through the main thermocline. *J. Phys. Oceanogr.*, **6,** 766–774.

Sanford, T. B., R. G. Drever and J. H. Dunlap, 1978: A velocity profiler based on the principles of geomagnetic induction. *Deep Sea Res.*, **25,** 183–200.

Shay, L. K., and R. L. Elsberry, 1985: Ocean current response to Hurricane Frederic. (in preparation).

Thompson, R. O. R. Y., 1977: Observations of Rossby waves near site D. *Progress in Oceanography,* Vol. 7, Pergamon, 135–162.

Webster, F., 1968: Observations of inertial period motions in the deep sea. *Rev. Geophys.*, **6,** 473–490.

Wunsch, C., 1968: On the propagation of internal waves up a slope. *Deep Sea Res.*, **15,** 251–258.

——, 1969: Progressive internal waves on slopes. *J. Fluid Mech.*, **35,** 131–144.

——, 1976: Geographical variability of the internal wave field: a search for sources and sinks. *J. Phys. Oceanogr.*, **6,** 471–481.

——, and R. Hendry, 1972: Array measurements of the bottom boundary layer and the internal wave field on the continental slope. *Geophys. Fluid Dyn.*, **4,** 101–145.